Response of the African Monsoon to Orbital Forcing and Ocean Feedbacks in the Middle Holocene

J. E. Kutzbach* and Z. Liu

Simulations with a climate model that asynchronously couples the atmosphere and the ocean showed that the increased amplitude of the seasonal cycle of insolation in the Northern Hemisphere 6000 years ago could have increased tropical Atlantic sea surface temperatures in late summer. The simulated increase in sea surface temperature and associated changes in atmospheric circulation enhanced the summer monsoon precipitation of northern Africa by more than 25 percent, compared with the middle Holocene simulation with prescribed modern sea surface temperatures, and provided better agreement with paleorecords of enhanced monsoons.

Earth's present climate is considerably different from that between about 12 and 5 thousand years ago (ka), in part because of differences in Earth's orbital parameters. Simulations with climate models have indicated that the orbital changes caused an increase in the amplitude of the seasonal cycle of solar radiation in the Northern Hemisphere, enhanced summertime land-ocean temperature contrasts, and thereby strengthened northern summer monsoons (*1–5*). Observations of northward extension of steppe and savanna vegetation and of lakes and wetlands have indicated that the Sahel and Sahara were considerably wetter in the early to middle Holocene than they are today (*6–9*). However, climate model simulations of these Holocene conditions have underestimated the degree of northward extension of monsoon rains even when surface albedo decreases and additional moisture recycling by the expanded area of vegetation (*7, 10*) and lakes and wetlands are taken into account (*11*). Here, we use a climate model simulation for 6 ka to show that the orbital forcing and initial enhancement of the monsoon circulation may have combined to produce changes in the sea surface temperature (SST) of the tropical North Atlantic that in turn caused further enhancement of precipitation in western North Africa.

In the climate model experiments, we used an atmospheric general circulation model (AGCM), Genesis 2, with an effective spatial resolution of 3.75° by 3.75° (*12*), and an ocean general circulation model (OGCM), MOM1, with an identical resolution (*13*). The control simulation of the AGCM (Control) was forced by modern-day insolation and modern, seasonally varying (prescribed) SST. Seasonally varying variables from a 5-year Control simulation (net solar radiation, downward-directed long-wave radiation, near-surface air temperature, specific humidity, and wind and wind stress) were then used to force a 500-year ocean simulation (Control Ocean). The ocean model provided the surface temperature required for calculating, in conjunction with the atmosphere variables, the surface energy fluxes. Ocean surface temperature was forced by these surface energy fluxes and by the flux associated with an additional restoring term that kept the simulated SSTs close to modern-day SSTs. In the subsequent ocean model simulation for 6 ka, the heat flux associated with the temperature restoring term was added as a prescribed flux correction.

A second AGCM experiment used incoming solar radiation appropriate for 6 ka (the experiment is denoted by R, for radiation) but was otherwise identical to the first experiment with prescribed modern SSTs. By forcing the flux-corrected ocean with the required atmospheric variables from R, we obtained an estimate of the seasonal response of the ocean to orbital forcing (R Ocean). We then calculated the differences in monthly SSTs between the R Ocean and Control Ocean simulations (ΔSST), added these differences to the prescribed modern SST fields to obtain a first approximation for the monthly SST field of 6 ka, and used the AGCM to simulate the seasonal atmospheric response to 6-ka insolation and the altered SSTs (R + ΔSST). We ignored possible changes in salinity associated with changes in freshwater flux by restoring salinity to modern values. The ocean model

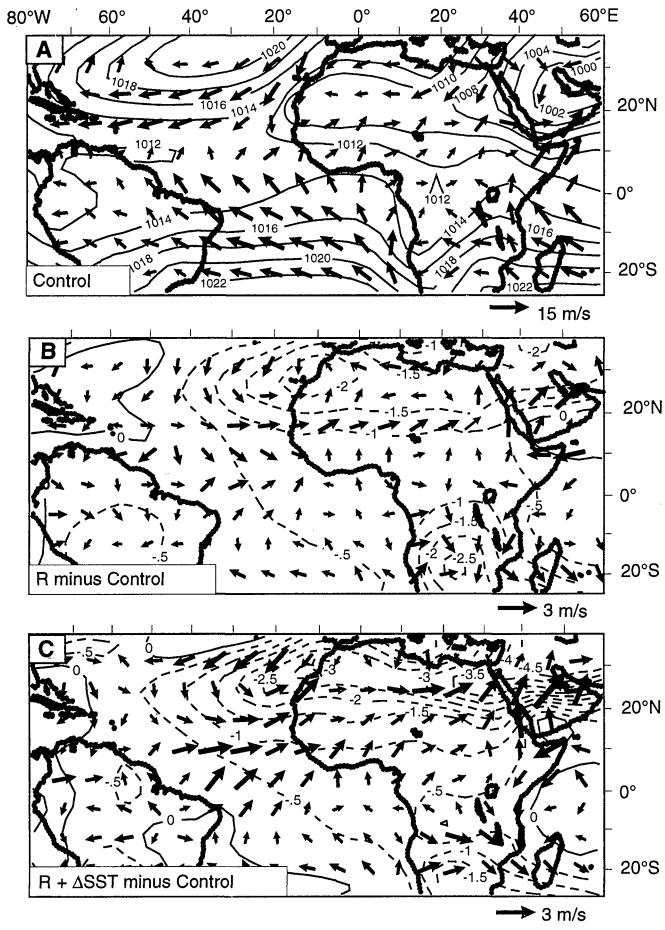

Fig. 1. Simulated sea-level pressure (in millibars) and surface wind (in meters per second) for JAS for (**A**) Control, (**B**) R minus Control, and (**C**) R + ΔSST minus Control. In (B) and (C), the regions of lowered sea-level pressure are shown with dashed contours, and the wind scale (departures from control) is increased by a factor of 5, as indicated by the reference vectors.

Center for Climatic Research, University of Wisconsin, Madison, WI 53706, USA.

*To whom correspondence should be addressed. E-mail: jek@facstaff.wisc.edu

did not include a sea-ice parameterization, and therefore, the sea-ice margin was kept at the control location in all of the AGCM experiments. The advantage of this asynchronous atmosphere-ocean coupling scheme, compared with a synchronous scheme, is that the effects of the altered atmosphere on the ocean (R Ocean minus Control Ocean) and the effects of the altered ocean on the atmosphere (R + ΔSST minus R) can be clearly isolated; the disadvantage is that these experiments may not necessarily capture the full response of a synchronously coupled model.

Although our simulations produced changes in all regions of the world, we focus here on changes in the Atlantic sector, as they impact the northern Africa summer monsoon (Fig. 1A). The changed atmospheric forcing (R minus Control) can potentially affect SST through changes in vertical energy flux (radiation, sensible heating, and evaporation) or changes in ocean dynamics (advection, upwelling, and diffusion). Our results show that two primary processes caused tropical Atlantic SSTs to increase: (i) Over the entire tropical Atlantic, the increased insolation (R minus Control) associated with late-summer perihelion increased the solar radiation absorbed at the surface of the ocean by 15 to 20 W/m^2 in northern summer and fall, and (ii) over the northern tropical Atlantic, evaporative heat loss from the ocean was reduced by about 5 to 10 W/m^2. This decrease in evaporative heat loss stems from the response of near-surface winds to the intensified heating of the atmosphere over northern Africa associated with the amplified seasonal cycle of insolation. This anomalous heating causes a lowering of surface pressure over and to the west of northern Africa (*14*, *15*) and an anomalous cyclonic circulation (Fig. 1B) that weakens the southern sector of the normal subtropical anticyclone at the ocean surface, thereby weakening the northern trade winds and reducing evaporative heat loss. These two increases in surface heat flux combine to produce an increase in northern tropical SSTs of about 0.2° to 0.4°C in summer and fall (Fig. 2). In the equatorial Atlantic, the temperature change is smaller. Temperature changes due to changes in ocean circulation are small compared with these more direct thermodynamic processes, at least in our coarse-resolution ocean model.

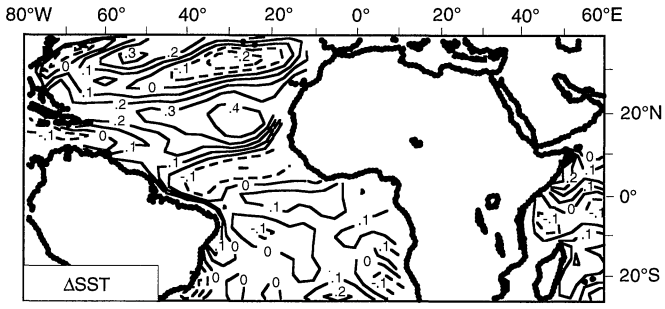

Fig. 2. Simulated change in SST (ΔSST) (in degrees Celsius) for JAS produced in the ocean model by orbitally forced changes in atmospheric forcing (R Ocean minus Control Ocean).

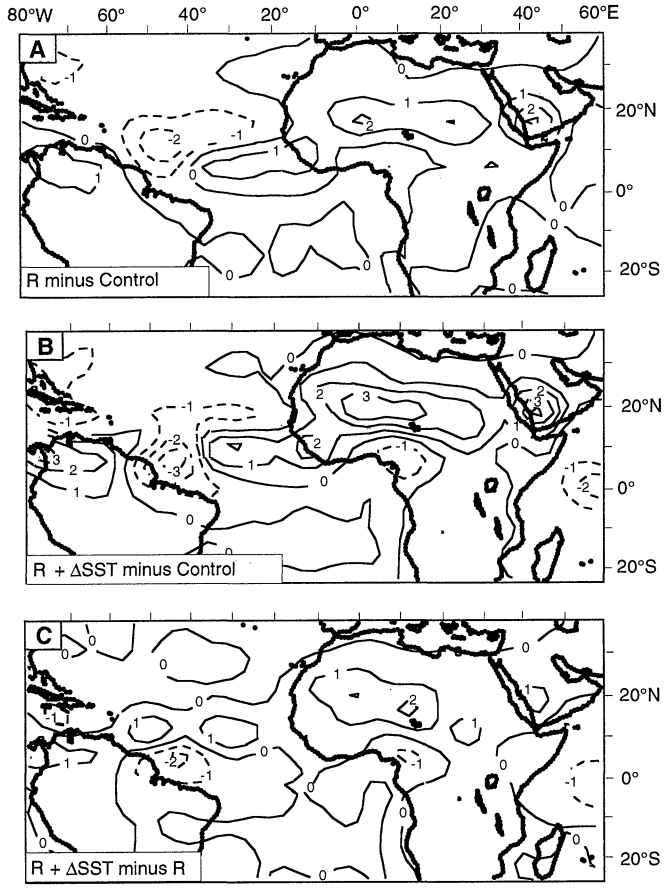

Fig. 3. Simulated change in JAS precipitation (in millimeters per day) for (**A**) R minus Control, (**B**) R + ΔSST minus Control, and (**C**) R + ΔSST minus R.

Precipitation increased in experiment R, compared with Control, over the tropical North Atlantic and northern Africa (Fig. 3A). Precipitation increased further in experiment R + ΔSST, compared with R, over both the warmer tropical North Atlantic and the western half of northern Africa (Fig. 3, B and C). This additional increase represents a positive feedback of the orbitally forced SST changes on the African monsoon. The simulated increase of precipitation over northern Africa in R + ΔSST, compared with R, is consistent with the observed increase of precipitation in the African Sahel in response to a warmer tropical North Atlantic, as deduced from studies of recent interannual variability (*16*, *17*). The simulated increase of precipitation over the ocean is associated with the increased SSTs; the warmer ocean surface reduces the climatological average meridional SST gradient and displaces northward the belt of low pressure associated with the Intertropical Convergence Zone. According to simplified dynamical models, the primary atmospheric response to the increased SST should be centered over and to the west of the region of anomalous heating (*14*), that is, over the ocean rather than to the east over West Africa. However, the anomalous westerly flow of moist air across the tropical Atlantic toward West Africa due to intensified heating over Africa (Fig. 1B) is further enhanced because of the local atmospheric response to the increased SST (Fig. 1C), and this anomalous flow combines with the strong gradient in specific humidity between the Atlantic Ocean and Africa to increase moisture transport. This moisture transport is in the form of a vertically deeper wedge of moist air (not shown in Fig. 1) that feeds the West African monsoon and causes additional increases in vertical motion, latent heat release, and precipitation and additional decreases in sur-

face pressure. In support of this interpretation, present-day observations show that in years with warmer northern tropical waters and enhanced rainfall in the Sahel, the wedge of moist air associated with the African summer monsoon is deeper and shifted north in response to increased southwesterly inflow along the African coast (*18*). This interpretation is also consistent with model-based studies of decadal climate variability in the tropical Atlantic (*19*).

The simulated flow response to anomalous heating therefore is more complex than the simplified dynamical response to a single prescribed heating perturbation (*14*). The increased complexity is a result of both forcing by multiple heat sources (intensified Asian monsoon, intensified African monsoon, and the warmer tropical Atlantic) and the presence of anomalous moisture advection from the Atlantic that further intensifies latent heat release and precipitation over West Africa (*20*).

The summer monsoon precipitation increased because of orbital forcing (R) as far north as 23°N and farther still to 30°N because of the combination of orbital forcing and changed SST (R + ΔSST) (Fig. 4). Moreover, the increases are especially large in the western Sahara (Fig. 3C), where earlier simulations without SST feedback were particularly deficient in orbitally forced monsoon extension (*10*). Averaged for 10° to 25°N and 17°W to 17°E, monsoon precipitation in July, August, and September (JAS) increased from 4.3 mm/day (Control) to 5.2 mm/day (R), a 17% increase, and to 6.4 mm/day (R + ΔSST), another 23% increase and an overall increase of about 50% compared with the control (Table 1). The simulation R + ΔSST brings wetter conditions as far north as is indicated by paleorecords of extended steppes, grasslands, lakes, and wetlands (*21*). The increase of precipitation in western North Africa resulting from the increased SST of the tropical Atlantic is comparable in magnitude with that associated with increased vegetation in sensitivity experiments based on land surface changes (*10*).

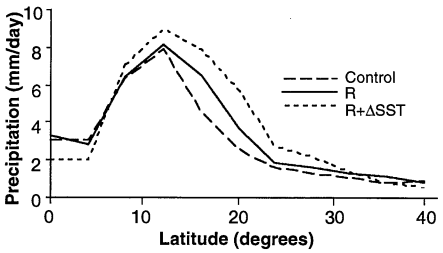

Fig. 4. Zonal average of JAS precipitation simulated over western North Africa (17°W to 17°E) for Control, R, and R + ΔSST.

Changes in equatorial Atlantic SSTs at the 23,000-year precession cycle have been intepreted in part as a response to orbitally forced variations in trade-wind– and monsoon-controlled equatorial divergence and upwelling (*22*). According to this argument, when perihelion occurs in northern summer, the increased low-level flow into the African continent reduces the strength of the trade winds and equatorial upwelling, and this decreased upwelling partially explains the large seasonal warming of the ocean surface of several degrees Celsius inferred from changes in planktonic assemblages in marine cores. The time series of planktonic-based SST changes correlates directly with the time series of precession-based insolation changes of the past 200,000 years. The expected magnitude of the direct response of SSTs to insolation changes is on the order of tenths of a degree Celsius, whereas the observed changes in SST through the extremes of the precession cycle are several degrees Celsius, leading to the inference that trade-wind–induced changes in equatorial upwelling explain the large SST signal (*22*). Although the trade winds are weakened in our AGCM simulation for 6 ka, in agreement with this inference, the upwelling response in the OGCM is small, perhaps because of the coarse resolution of the ocean model. Thus, the equatorial ocean temperature response in our simulation is small and comes primarily from the changed surface heat fluxes.

Mid-Holocene SST changes have been reported for the equatorial North Atlantic and for coastal areas of the subtropical North Atlantic (*23, 24*) but interpretation of these results is difficult because the temperature estimates vary widely within relatively small regions (*25*). There are no paleorecords currently available to verify the existence of the large area of slightly elevated tropical Atlantic ocean temperatures that was simulated by the OGCM (Fig. 2). Our simulation studies and the modern observational studies of interannual variability (*16, 17*) indicate that the African monsoon is highly sensitive to even small changes in SST over this region.

Although this report focuses on the simulation results for the tropical Atlantic and northern Africa, it will be important to examine possible ocean feedbacks on the atmospheric circulation in other regions during the mid-Holocene (*26*). Additional studies are also needed with either synchronous coupling between atmosphere and ocean models or iterative equilibrium asynchronous coupling between atmosphere and ocean models to assess whether or not the results of this sensitivity experiment approximate the steady-state solution.

A larger ocean feedback on the African monsoon might be expected at ~11 ka, during the early Holocene, or at ~125,000 ka, during the previous interglacial period, because perihelion occurred earlier in the northern summer than it did at 6 ka. This phase shift would have increased early summer insolation and produced a warming of the tropical Atlantic that would have been more in phase with the onset of the summer monsoon, compared with the late summer–early fall insolation increase that occurred at 6 ka.

Table 1. Climate variables from three climate model simulations (Control, R, and R + ΔSST) for JAS and for the annual average for the area 10° to 25°N and 17°W to 17°E, the western half of northern Africa. The changes in insolation reflect the changes in Earth's orbit. Precipitation rates in parentheses indicate the fractional change compared to Control. The decreased surface temperature is associated with the increased cloudiness and decreased sensible heat flux that accompany the enhanced monsoon rains.

Model simulation	Insolation (W/m^2)	Precipitation (mm/day)	Surface temperature (°C)
		JAS	
Control	436	4.3 (1.00)	28.5
R	457	5.2 (1.17)	28.1
R + ΔSST	457	6.4 (1.49)	26.3
		Annual average	
Control	397	1.7 (1.00)	25.5
R	396	1.8 (1.06)	24.8
R + ΔSST	396	2.6 (1.53)	24.5

REFERENCES AND NOTES

1. J. E. Kutzbach and B. L. Otto-Bliesner, *J. Atmos. Sci.* **39**, 1177 (1982).
2. J. E. Kutzbach and P. J. Guetter, *ibid.* **43**, 1726 (1986).
3. J. F. B. Mitchell, N. S. Grahame, K. H. Needham, *J. Geophys. Res.* **93**, 8283 (1988).
4. N. de Noblet, P. Braconnot, S. Joussaume, V. Masson, *Clim. Dyn.* **12**, 589 (1996).
5. N. M. J. Hall and P. J. Valdes, *J. Clim.* **10**, 3 (1997).
6. F. A. Street and A. T. Grove, *Nature* **261**, 385 (1976).
7. F. A. Street-Perrott, J. F. B. Mitchell, D. S. Marchand, J. S. Brunner, *Trans. R. Soc. Edinburgh* **81**, 407 (1990).
8. N. Petit-Maire and J. Riser, *Palaeogeogr. Palaeoclimatol. Palaeoecol.* **35**, 45 (1981).
9. D. Jolly, S. P. Harrison, B. Damnati, R. Bonnefille, *Quat. Sci. Rev.*, in press.
10. J. Kutzbach, G. Bonan, J. Foley, S. P. Harrison,

Nature **384**, 623 (1996).
11. M. Coe and G. Bonan, *J. Geophys. Res.* **102**, 11087 (1997).
12. S. L. Thompson and D. Pollard, *J. Clim.* **10**, 871 (1997).
13. R. C. Pacanowski, K. W. Dixon, A. Rosati, "The GFDL Modular Ocean Model Users Guide, Version 1" (GFDL Ocean Group Tech. Rep. 2, Geophysical Fluid Dynamics Laboratory, Princeton, NJ, 1991).
14. M. J. Rodwell and B. J. Hoskins, *Q. J. R. Meteorol. Soc.* **122**, 1385 (1996).
15. B. J. Hoskins and D. J. Karoly, *J. Atmos. Sci.* **38**, 1179 (1981).
16. S. Hastenrath, *Mon. Weather Rev.* **112**, 1097 (1984).
17. K. Wolter, *J. Clim.* **2**, 149 (1989).
18. P. J. Lamb, *Tellus A* **35**, 198 (1983).
19. P. Chang, L. Ji, H. Li, *Nature* **385**, 516 (1997).
20. This degree of monsoon enhancement was not found in earlier simulations of the climate of 6 or 9 ka that coupled an AGCM with a static mixed-layer ocean (*27*, *28*). Our analysis of these earlier experiments and other simulations confirms that the SSTs and low-level atmospheric winds of the control simulation are substantially biased by the lack of ocean dynamics and that this bias in the control alters the atmospheric response to orbital forcing. Cooler equatorial waters and a more humid continental surface may also strengthen the monsoon by increasing the south-to-north gradient of equivalent potential temperature in the boundary layer over western North Africa [E. A. B. Eltahir and C. Gong, *J. Clim.* **9**, 1030 (1996)]; however, the change of this gradient is small in our simulation. Warmer North Atlantic waters poleward of the tropics may also cause precipitation to increase in North Africa, based on the results of a climate model experiment [P. B. deMenocal and D. Rind, *J. Geophys. Res.* **98**, 7265 (1993)]; this linkage may occur in our stimulation as well.
21. P. Hoelzmann *et al.*, *Global Biogeochem. Cycles*, in press.
22. A. McIntyre, W. F. Ruddiman, K. Karlin, A. C. Mix, *Paleoceanography* **4**, 19 (1989); A. McIntyre and B. Molfino, *Science* **274**, 1867 (1996).
23. W. F. Ruddiman and A. C. Mix, in *Global Climates Since the Last Glacial Maximum*, H. E. Wright Jr. *et al.*, Eds. (Univ. of Minnesota Press, Minneapolis, 1993), pp. 94–124.
24. A. C. Mix, W. F. Ruddiman, A. McIntyre, *Paleoceanography* **1**, 43 (1986).
25. In the equatorial Atlantic, three core sites indicate warmer than present conditions, and 10 core sites indicate colder than present conditions with a range of anomalies between 2°C and −2°C for August (*23*). The sites indicating colder than present conditions do not agree in sign with the long time series site (*22*), which indicated warmer conditions coinciding with perihelion in northern summer. In the northern subtropics, a site near the Bahamas at 25°N shows a mid-Holocene maximum in annual temperature (an increase of ~0.5°C) (*24*). Adjacent to the African coast, 20° to 25°N, two core sites indicate warmer than present conditions, and three core sites indicate colder than present conditions with a range of anomalies between 1.5° and −2.9°C for August (*23*). As in the equatorial Atlantic, the intercore differences are relatively large.
26. Areas of particular future interest include the Arctic, where sea-ice cover almost certainly decreased (*3*, *27*, *28*); the Pacific, where there is evidence of changed El Niño–Southern Oscillation behavior [D. H. Sandweiss, J. B. Richardson III, E. J. Reitz, H. B. Rollins, K. A. Maasch, *Science* **273**, 1531 (1996)]; and the Indian Ocean, where changed upwelling in the Arabian Sea provided the first evidence for orbitally forced changes in monsoons [W. L. Prell, in *Milankovitch and Climate*, A. Berger *et al.*, Eds. (Reidel, Hingham, MA, 1984), pp. 349–366]. Changes in SSTs in these other ocean basins may also influence the climate of the Atlantic-African sector [(*17*); C. K. Folland, T. N. Palmer, D. E. Parker, *Nature* **320**, 602 (1986); T. N. Palmer, *ibid.* **322**, 251 (1986); S. Curtis and S. Hastenrath, *J. Geophys. Res.* **100**, 15835 (1995)]. On the basis of analogies with recent interannual variability [S. Hastenrath, *Climate and Circulation of the Tropics* (Reidel, Dordrecht, Netherlands, 1985)], the SST changes in the tropical Atlantic that were simulated at 6 ka could also lead to changes in the mid-Holocene climate of eastern tropical South America.
27. J. E. Kutzbach and R. G. Gallimore, *J. Geophys. Res.* **93**, 803 (1988).
28. J. E. Kutzbach *et al.*, *Quat. Sci. Rev.*, in press.
29. We thank W. Xu, R. Gallimore, and P. Behling for assistance with model simulations and graphics; M. Kennedy for preparing the manuscript; and S. L. Thompson and D. Pollard for allowing us to use the National Center for Atmospheric Research (NCAR) Genesis climate model. Supported by grants to the University of Wisconsin–Madison by the NSF's Climate Dynamics program and Earth System History program and by the U.S. Department of Energy. NCAR, which is sponsored by the NSF, provided computer resources.

23 July 1997; accepted 16 September 1997

Direct Observation of Cooling of Heme Upon Photodissociation of Carbonmonoxy Myoglobin

Yasuhisa Mizutani and Teizo Kitagawa*

The formation of vibrationally excited heme upon photodissociation of carbonmonoxy myoglobin and its subsequent vibrational energy relaxation was monitored by picosecond anti-Stokes resonance Raman spectroscopy. The anti-Stokes intensity of the ν_4 band showed immediate generation of vibrationally excited hemes and biphasic decay of the excited populations. The best fit to double exponentials gave time constants of 1.9 ± 0.6 and 16 ± 9 picoseconds for vibrational population decay and 3.0 ± 1.0 and 25 ± 14 picoseconds for temperature relaxation of the photolyzed heme when a Boltzmann distribution was assumed. The decay of the ν_4 anti-Stokes intensity was accompanied by narrowing and frequency upshift of the Stokes counterpart. This direct monitoring of the cooling dynamics of the heme cofactor within the globin matrix allows the characterization of the vibrational energy flow through the protein moiety and to the water bath.

Internal conversion processes after optical excitation or photoreactions leave the excited molecules or reaction products with excess energy. For small molecules the energy distributions in a molecule can be determined by transient absorption measurements (*1*), and these have provided considerable insight into intramolecular vibrational redistribution and vibrational cooling. For large molecules in condensed phases, however, the optical spectra are usually broad and featureless as a result of overlapping Franck-Condon transitions. For such systems, more direct monitoring of vibrational populations can be obtained, in principle, from time-resolved Raman (*2*, *3*) and infrared spectroscopy (*4*). Time-resolved resonance Raman (TR^3) spectroscopy is particularly suited for probing the vibrational state dynamics of colored molecules in solution phases. The ratio of the integrated areas of anti-Stokes and Stokes scattering, corrected to first order for reabsorption and cross section differences (*3*, *5*), is expected to yield the most direct information about relative vibrational populations. Here, we applied this technique to explore the heating and cooling dynamics of heme in the globin matrix upon photolysis of carbonmonoxy myoglobin (MbCO).

Myoglobin (Mb) is an oxygen-storage protein containing a heme prosthetic group (Fe^{II}-protoporphyrin IX). The heme is embedded within the globin and is linked to it through the proximal histidine. Small ligands such as O_2, CO, and NO bind reversibly to the sixth coordination site of Fe^{II}. These ligands are photodissociated on a femtosecond time scale by visible light (*6*–*8*). Although it was pointed out from subpicosecond time-resolved infrared (TRIR) absorption of D_2O (*9*) that some excess energy remains in the photodissociated heme shortly after the photolysis, there has been no direct observation of vibrationally excited populations of the photodissociated heme in the picosecond time regime. Therefore, we constructed a system for picosecond TR^3 measurements (*10*) and applied it to MbCO (*11*).

Stokes TR^3 difference spectra of photodissociated Mb with 2.3-ps resolution were obtained for various delay times of the probe pulse from the pump pulse (Fig. 1). The fraction of photolyzed MbCO was estimated from the intensity loss of the Raman bands of MbCO to be about 30%. The TR^3 spectrum in the 600 to 1500 cm^{-1} region for 0-ps delay (Fig. 1) shows bands arising from the in-plane vibrations of heme at 1351, 1115, 781, and 672 cm^{-1}, which are assigned to ν_4, ν_5, ν_{32}, and ν_7, respectively (*12*). These bands exhibited appreciable narrowing and frequency up-

Institute for Molecular Science, Okazaki National Research Institutes, Myodaiji, Okazaki 444, Japan.

*To whom correspondence should be addressed. E-mail: teizo@ims.ac.jp